Fracture Mechanics of Concrete Structures
Proceedings FRAMCOS-3
AEDIFICATIO Publishers, D-79104 Freiburg, Germany

STRESS ANALYSIS OF CONCRETE MATERIAL BASED ON GEOMETRICALLY ACCURATE FINITE ELEMENT MODELING

G. Nagai
Department of Environmental Physics and Engineering, Interdisciplinary Graduate School of Science and Engineering, Tokyo Institute of Technology, Japan
T. Yamada
Department of Architecture, Faculty of Engineering, Science University of Tokyo, Japan
A. Wada
Structural Engineering Research Center, Tokyo Institute of Technology, Japan

Abstract
This work proposes a stress analysis procedure for concrete material using a real digital image to generate a geometrically accurate finite element model of coarse aggregates and mortar. After illustrating the image digitizing and processing procedure, we present a three-dimensional linear analysis using the standard eight-node trilinear element of cubic shape. We also propose a mixed finite element that models cracks along the interfaces between coarse aggregates and mortar. These interfaces are defined by the digital sub-image embedded in the mixed element.
Key words: Digital image, composite material, mixed finite element

1 Introduction

Concrete material is a quasi-brittle material due to tensile failure. The mechanical behavior of a macroscopic concrete structure under tensile loading has been explained by fracture mechanics based on the assumption of a homogeneous material. However, for compressive loading, it is essential to consider local tensile failures resulting from the

heterogeneity of the material. To accurately model such local failures in a numerical analysis, the material must be dealt with as a composite material. In this study, we assume that concrete material has a two-phase structure consisting of coarse aggregates and mortar. Because of the existence of more microscopic constituents such as fine aggregates and cement paste, it is appropriate to call the two-phase structure a *mesoscopic* model.

In the numerical analysis of the mesoscopic structure, the geometric model defines the shapes of coarse aggregates and their positions without any overlapping, and the corresponding finite element mesh is generated. This procedure, especially in the three-dimensional (3-D) case, results in the following problems.

1. There are too many geometric modeling parameters to be defined. Even if random numbers are used, the modeling accuracy is another problem.
2. Coarse aggregates in the mesoscopic structure usually occupy 35~45% of the volume. Therefore, it is difficult for almost all the algorithms to generate a good finite element mesh with the boundaries of tiled elements fitted to the interfaces between aggregates and mortar (we refer to this as *fitted mesh*).

These problems can be overcome by directly using a digital image of the real concrete material. A digital image consists of small elements called *pixels* (picture cells) in the 2-D case or *voxels* (volume cells) in the 3-D case. If one pixel (voxel) is regarded as one finite element, the domain can be decomposed into exactly the same elements in shape. That is, all the mesh generation procedures can be replaced by digital image processing. We refer to such a digital image-based mesh as a *digital mesh*.

This original concept was proposed by S. J. Hollister and N. Kikuchi (1994) in the field of biomechanics. They applied it to the 3-D stress analysis of bone tissue, whose structure is too complicated to generate a fitted mesh. It was reported that its digital image was reconstructed by image scanning such as X-ray computed tomography.

This work proposes a stress analysis procedure for concrete material using a digital mesh. Section 2 briefly presents a digital image processing procedure and a 3-D linear analysis using an eight-node trilinear element of cubic shape. See also G. Nagai et al. (1998), where this is reported in detail. Section 3 proposes a new mixed finite element using an embedded digital sub-image that can model the cracks along the interface between coarse aggregates and mortar.

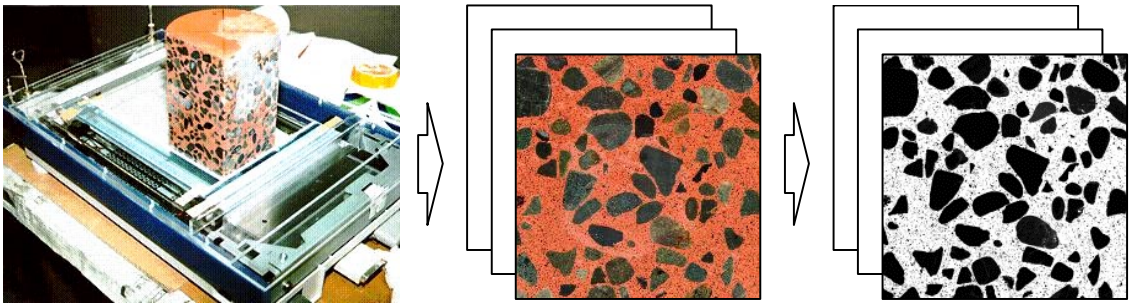

Fig. 1. Image digitizing and processing procedure

2 Application of digital mesh to concrete material

2.1 Image digitizing and processing as finite element modeling

A 3-D image can be obtained by binding a sequential set of 2-D sectional images. Physical destruction is the easiest way to obtain the sections of concrete material, and repetition of scraping can produce a sequential set. Accordingly, our digitizing procedure comprises repetition of the following: scrape a concrete specimen with a diamond scraper and acquire its sectional image by digitizing with a color flatbed scanner for PC. The cement paste in this specimen was colored with red Fe_2O_3 pigment for easy image processing, since concrete material is usually

Table 1. Material properties for mesoscopic structure

Material	Young's modulus (MPa)	Poisson's ratio
Coarse aggregate	5.3×10^4	0.15
Mortar	2.4×10^4	0.19

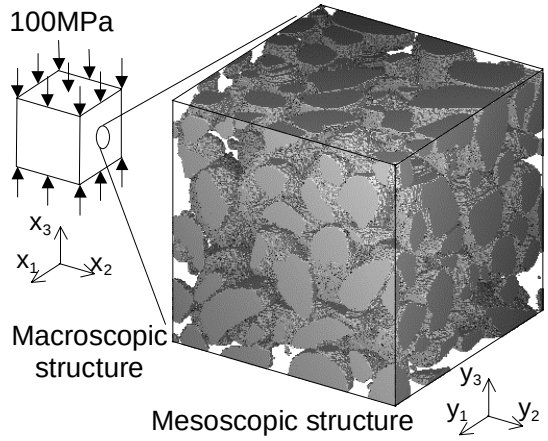

Fig. 2. Finite element model

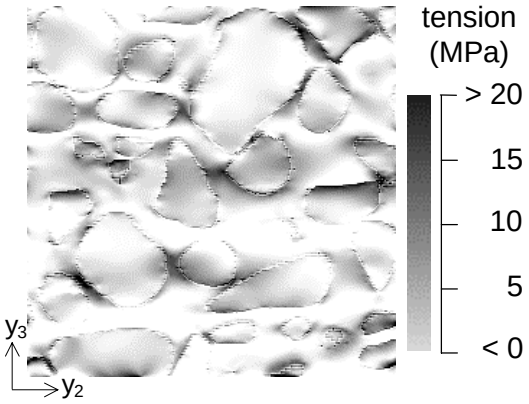

Fig. 3. Maximum principal stress in the center of y_2-y_3 section

grayish.

The digital image processing procedure is illustrated in Fig. 1. Based on the assumption of a two-phase (coarse aggregate and mortar) material, fine aggregates in the mortar are deleted from the images. Fine aggregate is so much smaller than coarse aggregate that the digital images can be processed independently in each 2-D section. After some operations, a 3-D grayscale image is obtained. Finally, a 3-D binary image in which the part comprising the coarse aggregates is marked 1 and the rest is marked 0 is obtained by thresholding of the grayscale image. This is equivalent to the digital mesh. If another mesh is required, it can be obtained by changing the resolution of the grayscale image.

2.2 Linear analysis of mesoscopic structure

This section presents an example calculated by the homogenization method. The homogenization method is derived from a mathematical theory based on the two-scale asymptotic expansion with respect to the displacement function. It is a remarkable theory in the field of composite materials (for example, see G. M. Guedes and N. Kikuchi (1990)).

Coarse aggregates in the mesoscopic structure, consisting of 256^3 elements (about 50 millions degrees of freedom) cut arbitrarily from the 3-D binary image, is shown in Fig. 2. Material properties for the

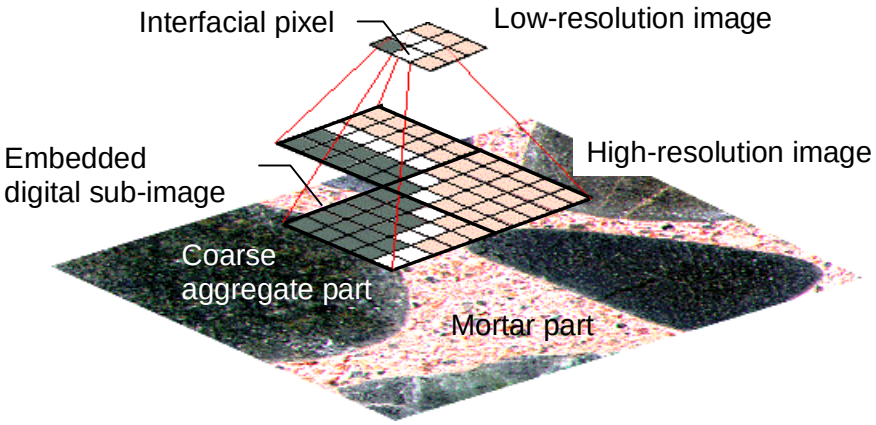

Fig. 4. Tree-structured hierarchical digital image

mesoscopic structure are given in table 1. The homogenization method is used to calculate the homogenized macroscopic elastic modulus and the stress in the mesoscopic structure. In this case, the macroscopic modulus is

$$\begin{bmatrix} 3.826 & 0.793 & 0.793 & -0.003 & 0.001 & 0.002 \\ 0.793 & 3.823 & 0.792 & -0.002 & -0.003 & 0.000 \\ 0.793 & 0.792 & 3.824 & 0.001 & -0.004 & 0.001 \\ -0.003 & -0.002 & 0.001 & 1.513 & 0.001 & -0.002 \\ 0.001 & -0.003 & -0.004 & 0.001 & 1.511 & 0.000 \\ 0.002 & 0.000 & 0.001 & -0.002 & 0.000 & 1.512 \end{bmatrix} (\text{x } 10^4 \text{ MPa}). \quad (1)$$

When a uni-axial 100 MPa compressive load is applied to the macroscopic structure, the maximum principal stress in the mesoscopic structure is as shown in Fig. 3.

3. Embedding of digital sub-image in digital mesh

The digital mesh has a lot of practical advantages for finite element modeling. However, it has several disadvantages in a precise simulation of non-linear behavior. For example, because of the nature of the digital image, the digital mesh causes a jagged approximation on the interface between coarse aggregate and mortar. Therefore, it needs to be fine, thus requiring many degrees of freedom. Furthermore, it can not model cracks along the interfaces.

In this section, as illustrated in Fig. 4, a concept of tree-structured hierarchical digital images is employed for the low-resolution interfacial pixels. High-resolution images are converted to low-resolution images

except for the interfacial pixels. The digital sub-images, which consist of the high-resolution pixels, are embedded in the interfacial pixels.

Now let us consider the interfacial pixels as mixed finite elements which can capture the strain discontinuity mode derived from the existence of different materials and the displacement discontinuity mode derived from the cracks along the interfaces. The other pixels are still regarded as the standard finite elements. The following illustrates the 2-D case, but the 3-D case is easily derived from it.

3.1 Approximation of interfacial finite element

The mixed finite element developed for the digital mesh is based on the approaches by J. Oliver (1996) and R. Larsson et al. (1995). The major differences between theirs and ours are the use of rectangular elements, the existence of different materials, and the fact that the crack direction has already been determined. This mixed element is an application of the assumed enhanced strain (AES) method formulated by J. C. Simo and M. S. Rifai (1990). The AES method has the feature of strain enrichment, i.e.

$$\varepsilon_e = \underbrace{\varepsilon_{ce}}_{\text{compatible}} + \underbrace{\tilde{\varepsilon}_e}_{\text{enhanced}} \tag{2}$$

where, the subscript e denotes the element number. The compatible strain ε_{ce} is interpolated by using a standard bilinear shape function, i.e.

$$\varepsilon_{ce} = B_e u_e \tag{3}$$

where, u_e is the nodal displacement.

The geometric parameters can be estimated from the sub-image shown in Fig. 5. However, the digital representation is not suitable for our formulation. Therefore, as shown in Fig. 6, an idealized approximation of the interface is considered. Here, the element Ω_{be} is split into three parts, namely Ω_{be}^{-}, Ω_{be}^{+}, and S_{be}. $|\cdot|$ denotes the area of the region. S_{be} is the thin band whose center is the idealized straight interface S_e. Its width and length are k_e and l_{Se}, respectively. The unit normal vector of the idealized interface S_e is $n_e = (n_{xe}, n_{ye})$.

We set the enhanced strain as

$$\tilde{\varepsilon}_e = G_{Re} u_{Re} + G_{He} u_{He} \tag{4}$$

$$G_{Re} = \left(H_{Se} - \left|\Omega_{be}^{+} \cup S_{be}^{+}\right| \Big/ \left|\Omega_{be}\right|\right) N_e \,, \quad G_{He} = \left(\delta_{Se} - l_{Se} \Big/ \left|\Omega_{be}\right|\right) N_e \tag{5}$$

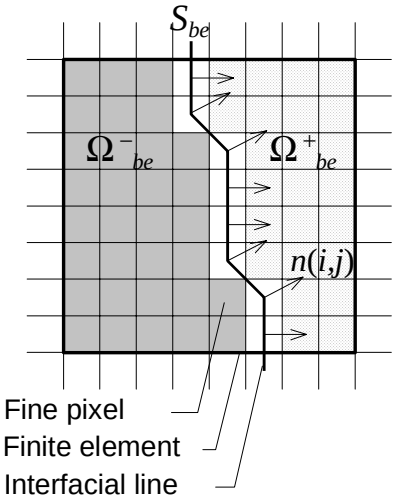

$$k_e = |S_{be}| / l_{Se}$$

$$n_e = \text{average}(n(i,j))$$

Fig. 5. Definition of geometric parameters in element

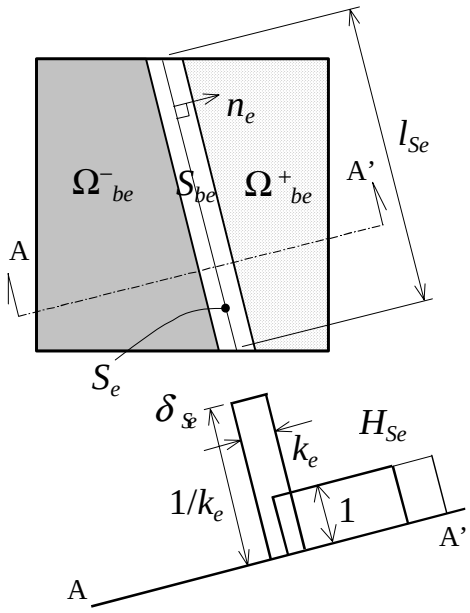

Fig. 6. Finite element approximation

$$N_e = \begin{bmatrix} n_{xe} & 0 \\ 0 & n_{ye} \\ n_{ye} & n_{xe} \end{bmatrix} \tag{6}$$

$$H_{Se} = \begin{cases} 0 & x \in \Omega^-_{be} \cup S^-_{be} \\ 1 & x \in \Omega^+_{be} \cup S^+_{be} \end{cases}, \quad \delta_{Se} = \begin{cases} 0 & x \in \Omega^-_{be} \cup \Omega^+_{be} \\ 1/k_e & x \in S_{be} \end{cases} \tag{7}$$

where, u_{Re} and u_{He} are the displacement gradient jump derived from the existence of different materials and the displacement jump derived from the crack, respectively. H_{Se} is the multi-dimensional version of Heaviside function, and δ_{Se} is the approximated multi-dimensional version of Derac's delta function in the sense of $\delta_{Se} k_e = 1$.

In the AES, the following equations must be satisfied so that the element passes the patch test.

$$\int_{\Omega_{be}} G_{Re}\, d\Omega = 0\,, \quad \int_{\Omega_{be}} G_{He}\, d\Omega = 0 \tag{8}$$

As a result of the formulation, the element stiffness equation can be expressed as

$$\int_{\Omega_{be}} \begin{bmatrix} B_e^T C B_e & B_e^T C G_{Re} & B_e^T C G_{He} \\ & G_{Re}^T C G_{Re} & G_{Re}^T C G_{He} \\ \text{sym.} & & G_{He}^T C G_{He} \end{bmatrix} d\Omega \begin{Bmatrix} u_e \\ u_{Re} \\ u_{He} \end{Bmatrix} = \begin{Bmatrix} f_e \\ 0 \\ 0 \end{Bmatrix} \tag{9}$$

This element stiffness can be assembled by the standard finite element procedure via the static condensation.

3.2 Numerical integration

The material modulus function C_e in each interfacial element can be defined as

$$C_e = C_e^- + \left(C_e^+ - C_e^-\right) H_{Se} + \left(C_{Se} - C_e^-\right) k_e \delta_{Se}^- + \left(C_{Se} - C_e^+\right) k_e \delta_{Se}^+ \tag{10}$$

where, C_e^-, C_e^+, and C_{Se} are constants defined in Ω_{be}^-, Ω_{be}^+, and S_{be}. δ_{Se}^-, and δ_{Se}^+ are the split functions of δ_{Se} at the center S_e, i.e. $\delta_{Se}^- + \delta_{Se}^+ = \delta_{Se}$.

Expanding Eq. (9) with respect to H_{Se}, δ_{Se}^-, δ_{Se}^+, the element stiffness K_{be} can be approximated as

$$K_{be} = \begin{cases} I(\Omega_{be}) + I(\Omega_{be}^+) + I(S_{be}) & \left|\Omega_{be}^-\right| > \left|\Omega_{be}^+\right| \\ I(\Omega_{be}) + I(\Omega_{be}^-) + I(S_{be}) & \left|\Omega_{be}^-\right| \le \left|\Omega_{be}^+\right| \end{cases} \tag{11}$$

where, $I(\cdot)$ denotes a numerical integration with respect to the region $(\cdot)$. This integration is estimated by using the embedded digital sub-image shown in Fig. 5.

3.3 Numerical experiment

A simple model is used to check the performance of the present mixed finite element. The model shown in Fig. 7, which consists of 80^2 high-resolution pixels, is decomposed into 10^2 finite elements. The Young's modulus for the interfaces is made much smaller than those for the others to model the tensile failures in a non-linear simulation. The mixed element is used for the elements containing the interface, and the standard four-node bilinear element is used for the other elements. This mesh is shown in Fig. 8.1. In this case, one digital sub-image consisting of 8^2 fine pixels is embedded in one mixed element. To compare the performance, the same mesh for which only the standard element is used, is shown in

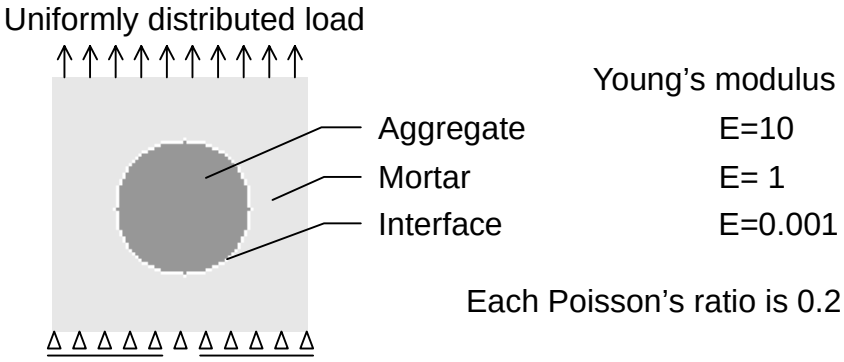

Fig. 7. Simple 80^2 pixels model

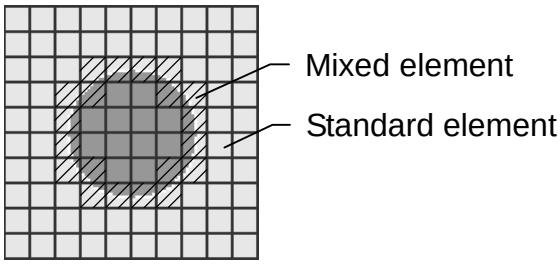

Fig. 8.1. Mixed element mesh

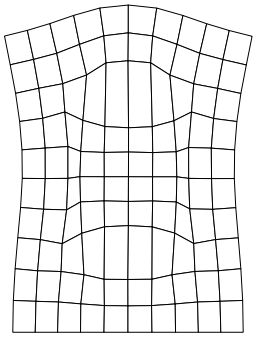

Fig. 8.2. Mesh deformation

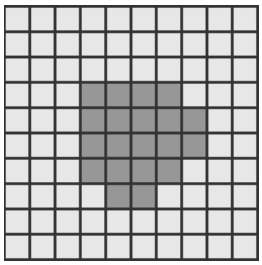

Fig. 9.1. Standard element mesh

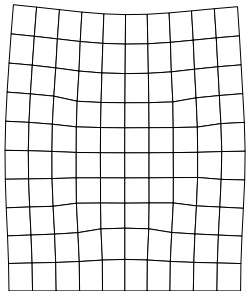

Fig. 9.2. Mesh deformation

Fig. 9.1. This mesh can not represent the interface.

When a uniformly distributed load is applied to the model, its mesh deformations are as shown in Fig. 8.2 and 9.2, respectively. This comparison shows that the mixed element can model the cracks along interfaces.

4. Concluding remarks

We have proposed direct use of digital images for finite element modeling. This digital-image-based mesh simply and precisely reflects the structural geometry of concrete material. However, it has the disadvantages that many elements are required and the cracks along interfaces can not be modeled. Therefore, we have also proposed a new mixed finite element to overcome these disadvantages.

References

G. M. Guedes and N. Kikuchi (1990) Preprocessing and postprocessing for materials based on the homogenization method with adaptive finite element methods, **Comp. Meth. Appl. Mech. Eng.**, 83 143-198

G. Nagai, T. Yamada, and A. Wada (1998) On a finite element procedure based on the real 3-dimensional image for concrete materials, **J. Struc. and Cons. Eng. (Trans. AIJ)**, 509 (to appear in Japanese)

J. C. Simo and M. S. Rifai (1990) A class of mixed assumed strain methods and the methods of incompatible modes, **Int. J. Num. Meth. Eng.**, 29, 1595-1638

J. Oliver (1996) Modelling strong discontinuities in solid mechanics via strain softening constitutive equations. Part II: numerical simulation, **Int. J. Num. Meth. Eng.**, 39, 3601-3623

R. Larsson, K. Runesson, and M. Akesson (1995) Embedded localization band on regularized strong discontinuity, in **4th Int. Conf. on Computational Plasticity** (eds D. R. J. Owen et al.), Pineridge Press, Swansea, 599-610

S. J. Hollister and N. Kikuchi (1994) Homogenization theory and digital imaging: a basis for studying the mechanics and design principles of bone tissue, **Biotech. Bioeng.**, 43, 586-596